$[Cu(tn)]_3[W(CN)_8]_2{\cdot}3H_2O$ and $[Cu(pn)]_3[W(CN)_8]_2{\cdot}3H_2O$: Two Novel Cu(II)−W(V) Cyano-Bridged Two-Dimensional Coordination Polymers with Metamagnetism

Dong-feng Li,*,† Li-min Zheng,† Xin-yi Wang,‡ Jin Huang,† Song Gao,*,‡ and Wen-xia Tang†

State Key Laboratory of Coordination Chemistry, Coordination Chemistry Institution, Nanjing University, Nanjing 210093, P. R. China, and State Key Laboratory of Rare Earth Materials and Applications, College of Chemistry and Molecular Engineering, Peking University, Beijing 100871, P. R. China

Received January 10, 2003

Two novel 3d−5d Cu(II)−W(V) cyano-bridged compounds, $[Cu(tn)]_3[W(CN)_8]_2{\cdot}3H_2O$ (**1**) and $[Cu(pn)]_3[W(CN)_8]_2{\cdot}3H_2O$ (**2**), where tn is 1,3-diaminopropane and pn is 1,2-diaminopropane, have been synthesized and characterized structurally and magnetically. The X-ray analyses of the two complexes reveal that they exhibit two-dimensional layer structures with the following crystal data: space group $P2_1/c$, $a = 24.459(5)$ Å, $b = 9.6426(19)$ Å, $c = 18.037(4)$ Å, $\beta = 90.45(3)°$, $V = 4253.9(15)$ Å^3, $Z = 4$ for **1**; and space group $P2_1/c$, $a = 24.126(5)$ Å, $b = 9.8889(19)$ Å, $c = 18.077(3)$ Å, $\beta = 90.204(4)°$, $V = 4312.9(14)$ Å^3, and $Z = 4$ for **2**. Magnetic properties of the two compounds have also been investigated. Both show typical metamagnetic behavior. The critical field at which the interlayer antiferromagnetic ground-state switches to a ferromagnetic state is ~1.25 T for **1** and 0.35 T for **2** at 1.8 K.

Introduction

There has been continuous interest in the molecule-based magnetic material of cyano-bridged bimetallic assemblies because of their remarkable magnetic, magnetic−optical, and optoelectronic properties.[1,2] Some notable results for Prussian Blue analogues have been reported, for example, the discovery of a molecule-based magnet, $KV^{II}[Cr^{III}(CN)_6]{\cdot}2H_2O$, with long-range magnetic ordering at T_C as high as 376 K (103 °C).[2] To exploit new molecule-based magnetic material, the paramagnetic hepta/octacyanometalates ($[Mo^{III}(CN)_7]^{4-}$, $[Mo^V(CN)_8]^{3-}$, $[W^V(CN)_8]^{3-}$) have been chosen as building blocks to construct novel bimetallic cyano-bridged assemblies for the more diffuse d orbital of the central 4d/5d metal ions and their versatility in coordination number and geometry.[3−6] By the self-assembly of these anion species with 3d cationic complex paramagnetic constituent blocks, a few 1-D chains,[4] and 2-D[5] and 3-D[6] polymers based on octacyanometalates ($[M(CN)_8]^{3-}$, M is Mo, W) have been obtained recently, which exhibit long-range ferromagnetic ordering in the range of 2−54 K. To our knowledge, no polymer derived from octacyanometalates showing metamagnetism has been well documented till now. Here, we present the structures and magnetic properties of two 2-D Cu(II)−W(V) cyano-bridged compounds, $[Cu(tn)]_3[W(CN)_8]_2{\cdot}3H_2O$ (**1**) and $[Cu(pn)]_3[W(CN)_8]_2{\cdot}3H_2O$ (**2**) (tn is 1,3-diaminopropane and pn is 1,2-diaminopropane), which show metamagnetic behavior at low temperature.

Experimental Section

Materials and Methods. All the starting materials were reagent grade and used as received. $K_3[W(CN)_8]{\cdot}H_2O$ was prepared according to published procedures.[7] The elemental analyses were performed on a Perkin-Elmer 240C elemental analyzer. Infrared spectra were measured on a Bruker Vector 22 FT−IR instrument from KBr pellets. The magnetic susceptibilities and field dependence of magnetization up to 7 T at 1.8 K were obtained on polycrystalline samples using a Model MagLab System 2000 magnetometer. The experimental susceptibilities were corrected for the sample holder and the diamagnetism contributions were estimated from Pascal's constants.[8]

---

* Corresponding authors. E-mail: chem1121@nju.edu.cn (D.L); or gaosong@pku.edu.cn (S.G.). Fax: +86-25-331-4502.

† Nanjing University.

‡ Peking University.

(1) For example: Mallah, T.; Thiébaut, S.; Verdaguer, M.; Veillet, P. *Science* **1993**, *262*, 1554. Ently, W. R.; Girolami, G. S. *Science* **1995**, *268*, 397. Verdaguer, M. *Science* **1996**, *272*, 698. Sato, O.; Iyoda, T.; Fujishina, A.; Hashimoto, K. *Science* **1996**, *271*, 49; Sato, O.; Iyoda, T.; Fujishina, A.; Hashimoto, K. *Science* **1996**, *272*, 704.

(2) Holmes, S. M.; Girolami, G. S. *J. Am. Chem. Soc.* **1999**, *121*, 5593, and references therein.

(3) Larionova, J.; Clérac, R.; Sanchiz, J.; Kahn, O.; Golhen, S.; Ouahab, L. *J. Am. Chem. Soc.* **1998**, *120*, 13088. Larionova, J.; Kahn, O.; Golhen, S.; Ouahab, L.; Clérac, R. *J. Am. Chem. Soc.* **1999**, *121*, 3349. Kaur Sra, A.; Andruh, M.; Kahn, O.; Golhen, S.; Ouahab, L.; Yakhmi, J. V. *Angew. Chem., Int. Ed.* **1999**, *38*, 2606. Larionova, J.; Gross, M.; Pilkington, M.; Andres, H.; Stoeckli-Evans, H.; Güdel, H. U.; Decurtins, S. *Angew. Chem., Int. Ed.* **2000**, *39*, 1605. Chibotaru, L. F.; Mironov, V. S.; Ceulemans, A. *Angew. Chem., Int. Ed.* **2001**, *40*, 4429, and references therein.

(4) Li, D.-f.; Gao, S.; Zheng, L.-m.; Tang, W.-x. *J. Chem. Soc., Dalton Trans.* **2002**, 2805.

(5) Podgajny, R.; Korzeniak, T.; Balanda, M.; Wasiutynski, T.; Errington, W.; Kemp, T. J.; Alcock, N. W.; Sieklucka, B. *Chem. Commun.* **2002**, 1138.

(6) Li, D.-F.; Gao, S.; Zheng, L.-M.; Sun, W.-Y.; Okamura, T.-a.; Ueyama, N.; Tang, W.-X. *New J. Chem.* **2002**, *26*, 485. Zhong, Z. J., Seino, H., Mizobe, Y., Hidai, M., Verdaguer, M., Ohkoshi, S.; Hashimoto, K. *Inorg. Chem.* **2000**, *39*, 5095.

(7) Baadsgaard, H.; Treadwell, W. D. *Helv. Chim. Acta* **1955**, *38*, 1669.

10.1021/cm030144n CCC: $25.00

Table 1. Crystallographic Data for Compounds 1 and 2

compound	1	2
formula	$C_{25}H_{36}N_{22}O_3Cu_3W_2$	$C_{25}H_{36}N_{22}O_3Cu_3W_2$
M	1251.08	1251.08
crystal system	monoclinic	monoclinic
space group	$P2_1/c$	$P2_1/c$
a/Å	24.459(5)	24.126(5)
b/Å	9.6426(19)	9.8889(19)
c/Å	18.037(4)	18.077(3)
β/deg	90.45(3)	90.204(4)
V/Å^3	4253.9(15)	4312.9(14)
Z	4	4
D_c/g cm^{-3}	1.953	1.927
F(000)	2396	2396
μ(Mo Kα)/mm^{-1}	6.919	6.824
goodness-of-fit on F^2	1.004	1.003
R1, wR2 [$I > 2\sigma(I)$]	0.0334, 0.0778	0.0402, 0.0767
(all data)	0.0435, 0.0803	0.0560, 0.0795

Table 2. Selected Bond Lengths [Å] and Angles [deg] for Compound 1^{a}

Cu(1)−N(10)	1.999(6)	Cu(1)−N(18)	1.993(5)
Cu(1)−N(8)^{i}	2.010(6)	Cu(1)−N(17)	1.996(6)
Cu(1)−N(4)	2.238(5)	Cu(2)−N(5)	2.020(6)
Cu(2)−N(9)	2.014(6)	Cu(2)−N(21)	1.962(5)
Cu(3)−N(6)^{ii}	2.003(6)	Cu(2)−N(22)	1.963(5)
Cu(3)−N(16)	1.998(5)	Cu(3)−N(12)^{iii}	2.222(5)
Cu(3)−N(19)	1.998(5)	Cu(3)−N(20)	1.975(6)
N(10)−Cu(1)−N(8)^{i}	89.6(2)	N(18)−Cu(1)−N(17)	93.6(2)
N(18)−Cu(1)−N(4)	98.3(2)	N(18)−Cu(1)−N(10)	87.7(2)
N(17)−Cu(1)−N(4)	90.8(2)	N(17)−Cu(1)−N(8)^{i}	89.1(2)
N(10)−Cu(1)−N(4)	89.5(2)	N(8)^{i}−Cu(1)−N(4)	106.4(2)
N(21)−Cu(2)−N(22)	93.7(2)	N(21)−Cu(2)−N(5)	88.6(2)
N(22)−Cu(2)−N(9)	89.6(2)	N(9)−Cu(2)−N(5)	88.9(2)
N(19)−Cu(3)−N(6)^{ii}	87.0(2)	N(20)−Cu(3)−N(19)	95.1(2)
N(16)−Cu(3)−N(6)^{ii}	88.1(2)	N(20)−Cu(3)−N(16)	86.5(2)
N(20)−Cu(3)−N(12)^{iii}	95.6(2)	N(16)−Cu(3)−N(12)^{iii}	104.6(2)
N(19)−Cu(3)−N(12)^{iii}	92.3(2)	N(6)^{ii}−Cu(3)−N(12)^{iii}	96.2(2)
C(4)−N(4)−Cu(1)	152.6(5)	C(8)−N(8)−Cu(1)^{v}	167.3(6)
C(10)−N(10)−Cu(1)	169.0(6)	C(5)−N(5)−Cu(2)	174.7(7)
C(12)−N(12)−Cu(3)^{vi}	151.1(5)	C(9)−N(9)−Cu(2)	174.5(7)
C(16)−N(16)−Cu(3)	162.5(6)	C(6)−N(6)−Cu(3)^{iv}	177.5(6)

^{a} Symmetry transformations used to generate equivalent atoms: ^{i} $x, y - 1, z$; ^{ii} $x, -y + {}^1/_2, z - {}^1/_2$; ^{iii} $x, -y - {}^1/_2, z - {}^1/_2$; ^{iv} $x, -y + {}^1/_2, z + {}^1/_2$; ^{v} $x, y + 1, z$; ^{vi} $x, -y - {}^1/_2, z + {}^1/_2$.

Table 3. Selected Bond Lengths [Å] and Angles [deg] for Compound 2^{a}

Cu(1)−N(3)	2.000(8)	Cu(1)−N(10)^{i}	1.997(7)
Cu(1)−N(15)	2.372(7)	Cu(1)−N(17)	1.998(7)
Cu(1)−N(18)	1.994(6)	Cu(2)−N(4)	1.984(7)
Cu(2)−N(13)	1.984(7)	Cu(2)−N(19)	1.969(7)
Cu(2)−N(20)	1.994(6)	Cu(3)−N(7)^{ii}	2.006(7)
Cu(3)−N(8)	2.291(7)	Cu(3)−N(21)	1.953(7)
Cu(3)−N(11)^{i}	1.956(7)	Cu(3)−N(22)	1.983(6)
N(3)−Cu(1)−N(18)	92.6(3)	N(10)^{i}−Cu(1)−N(3)	91.3(3)
N(10)^{i}−Cu(1)−N(17)	90.0(3)	N(10)^{i}−Cu(1)−N(15)	99.0(2)
N(3)−Cu(1)−N(15)	96.2(3)	N(17)−Cu(1)−N(18)	85.2(3)
N(17)−Cu(1)−N(15)	89.0(3)	N(18)−Cu(1)−N(15)	90.0(2)
N(4)−Cu(2)−N(13)	92.7(3)	N(4)−Cu(2)−N(19)	91.7(3)
N(13)−Cu(2)−N(20)	91.3(3)	N(19)−Cu(2)−N(20)	85.0(3)
N(11)^{i}−Cu(3)−N(21)	91.1(3)	N(22)−Cu(3)−N(21)	83.6(3)
N(11)^{i}−Cu(3)−N(7)^{ii}	91.2(3)	N(22)−Cu(3)−N(7)^{ii}	92.5(3)
N(22)−Cu(3)−N(8)	92.1(3)	N(11)^{i}−Cu(3)−N(8)	92.4(3)
N(7)^{ii}−Cu(3)−N(8)	103.4(3)	N(21)−Cu(3)−N(8)	95.2(3)
C(3)−N(3)−Cu(1)	177.2(8)	C(15)−N(15)−Cu(1)	148.6(6)
C(4)−N(4)−Cu(2)	169.4(7)	C(10)−N(10)−Cu(1)^{iv}	156.5(7)
C(7)−N(7)−Cu(3)^{iii}	168.7(8)	C(13)−N(13)−Cu(2)	166.7(8)
C(11)−N(11)−Cu(3)^{iv}	175.6(7)	C(8)−N(8)−Cu(3)	157.2(7)

^{a} Symmetry transformations used to generate equivalent atoms: ^{i} $x, -y + {}^3/_2, z - {}^1/_2$; ^{ii} $x, -y + {}^5/_2, z - {}^1/_2$; ^{iii} $x, -y + {}^5/_2, z + {}^1/_2$; ^{iv} $x, -y + {}^3/_2, z + {}^1/_2$.

Preparation of $[Cu(tn)]_3[W(CN)_8]_2\cdot 3H_2O$ (1). To an aqueous solution (80 cm^3) of $Cu(ClO_4)_2\cdot 6H_2O$ (0.444 g, 1.2 mmol) and 1,3-diaminopropane (tn; 0.05 mL, 1.2 mmol), $K_3[W(CN)_8]\cdot H_2O$ (0.422 g, 0.8 mmol) in 20 cm^3 of distilled water was added with stirring at room temperature. The resulting blue solution was allowed to stand for several days and dark blue platelet crystals were obtained. They were collected by suction filtration, washed with water, and dried in air. All the operations for the synthesis were carried out in the dark to avoid decompositions of $K_3[W(CN)_8]\cdot H_2O$. Yield: 0.66 g (66% based on W). Anal. Calcd for $C_{25}H_{36}N_{22}O_3Cu_3W_2$: C, 24.00; H, 2.90; N, 24.63%. Found: C, 24.24; H, 2.98; N, 24.42%. IR (cm^{-1}, KBr disk): $\nu_{C\equiv N}$ 2189m, 2150s.

Preparation of $[Cu(pn)]_3[W(CN)_8]_2\cdot 3H_2O$ (2). This assembly was prepared as blue crystals in a way similar to that of **1**, except for the use of 1,2-diaminopropane (pn) instead of tn. Anal. Calcd for $C_{25}H_{36}N_{22}O_3Cu_3W_2$: C, 24.00; H, 2.90; N, 24.63%. Found: C, 24.15; H, 2.94; N, 24.50%. IR (cm^{-1}, KBr disk): $\nu_{C\equiv N}$ 2203s, 2188s, 2156s.

X-ray Crystallographic Analysis. Intensities data for the crystals of **1** and **2** were collected on a Bruker Apex SMART CCD system equipped with monochromated Mo−Kα radiation (λ = 0.71073 Å) at room temperature. The data integration and empirical absorption corrections were carried out by SAINT[9] and SADABS[10] programs, respectively. The structures were solved by direct methods and refined on F^2 using the SHELXTL suite of program.[11] All non-hydrogen atoms for the two complexes were refined anisotropically by full-matrix least squares. Hydrogen atoms were generated geometrically. For **1**, the atoms C23A, C23B and C25A, C25B are disordered, and the sofs were fixed at 0.5. The largest difference peak and hole in **1** are 1.793 and −2.000 e·Å^{-3}, within 1.0 Å from W1 and Cu2, respectively. Selected crystallographic data and structure determination parameters for the two complexes are given in Table 1.

Results and Discussion

Crystal Structures. The selected bond lengths and angles for complexes **1** and **2** are listed in Tables 2 and 3, respectively, and the molecular structures of the asymmetric units for the two coordination polymers are shown in Figure 1. For complex **1**, there are two $[W(CN)_8]^{3-}$ ions and three $[Cu(tn)]^{2+}$ cations together with three water molecules in the asymmetric unit. Each of the two W atoms is coordinated by eight CN groups in an irregular square antiprism with W−C distances ranging from 2.127(7) to 2.180(7) Å. Cu1 sphere can be described as a distorted square pyramidal geometry with the axial atom N4 and the equatorial coordinated atoms N8*A* N10, N17, and N18, in which N4, N8*A*, and N10 are from the cyanides of three adjacent $[W(CN)_8]$ moieties, and N17 and N18 are from an exogenous tn ligand (*A*: $x, y - 1, z$). Similarly, Cu3 is also in a distorted square pyramidal coordination environment, in which the axial position and two equatorial sites are occupied by three cyanides (N6*B*, N12*C*, and N16, *B*: $x, {}^1/_2 - y, {}^{-1}/_2 + z$; *C*: $x, {}^{-1}/_2 - y, {}^{-1}/_2 + z$) from adjacent $[W(CN)_8]$ moieties, and the other equatorial sites (N19, N20) are occupied by a tn ligand. The Cu2 atom presents a distorted CuN4 planar square arising from two nitrogen atoms (N21 and N22) of a tn ligand and two nitrogen atoms (N6 and N16) from adjacent CN groups. The axial Cu−N$_{ax}$ bonds for Cu1

---

(8) Kahn, O. *Molecular Magnetism*; VCH Publishers: New York, 1993.

(9) *SAINT*, Data Integration Software; Bruker AXS, Inc.: Madison, WI, 1997.

(10) Sheldrick, G. M. *SADABS*, Empirical Absorption Correction Program; University of Göttingen: Germany, 1996.

(11) Sheldrick, G. M. *SHELXTL*, Program for Crystal Structure Determinations; Siemens Industrial Automation Inc.: Madison, WI, 1997.

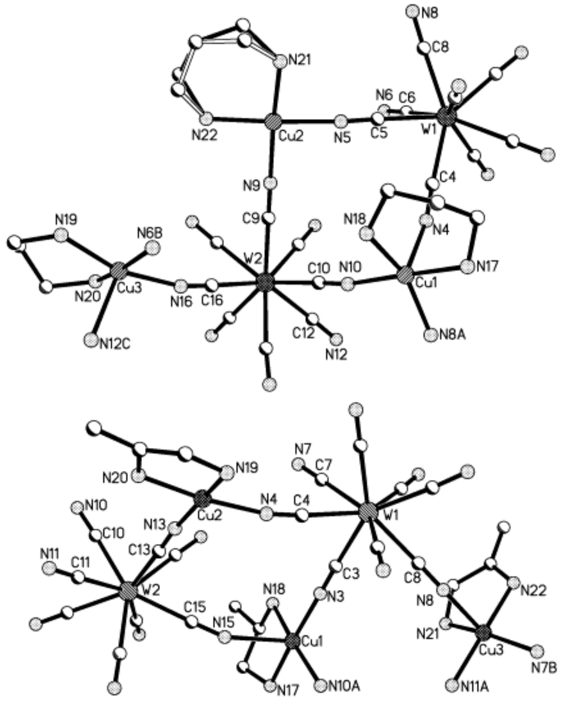

Figure 1. Molecular structures for complexes **1** (top) and **2** (bottom), showing the atomic labeling scheme. Codes of equivalent positions: *A* $x, y - 1, z$; *B* $x, {}^1/_2 - y, -{}^1/_2 + z$; *C* $x, -{}^1/_2 - y, -{}^1/_2 + z$ for **1**; *A* $x, {}^3/_2 - y, -{}^1/_2 + z$; *B* $x, {}^5/_2 - y, -{}^1/_2 + z$ for **2**.

and Cu3 [Cu1−N4 = 2.238(5), Cu3−N12*C* = 2.222(5) Å] are slightly longer than the equatorial $\mathrm{Cu-N_{eq}}$ bonds in the range of 1.993(5) to 2.010(6) Å. Consequently, for each W atom, there are four CN groups acting as bridging units and four others acting as terminals.

Through the bridging cyano groups (C4−N4, C5−N5, C9−N9, and C10−N10), W1, Cu1, W2, and Cu2 atoms are linked to form a twelve-membered tetrametallocycle $[\mathrm{Cu_2W_2(CN)_4}]$, while the Cu1, W2, W3, and W1 are also bridged to form a distorted square by four cyano groups (C10−N10, C12−N12, C6−N6, and C8−N8) (see Figure 2). As a result, the two twelve-membered rings share a same lateral (Cu1−N10−C10−W2) to form a "butterfly-like" motif. By sharing one vertex (W1), these "butterflies" are connected to each other to lead to one-dimensional infinite chains extended along the *b* axis (Figure 2). Furthermore, along the *c* axis, the one-dimensional infinite chains are united through the CN bridges between W2 and Cu3 in an alternate −A−B−A−B− pattern to construct the neutral two-dimensional layered structure as shown in Figure 2. The closest metal···metal distances in **1** are 5.215 Å for Cu3···W2 within the layer and 7.162 Å for Cu3···W2′ (′: $1 - x, -y, -z - 2$) between the layers.

Complex **2** has a structural features similar to those of **1**. The asymmetric unit consists of two $[\mathrm{W(CN)_8}]^{3-}$ ions, three $[\mathrm{Cu(pn)}]^{2+}$ cations, and three water molecules (Figure 1). The coordination environments of the W1, W2, Cu1, Cu2, and Cu3 metal centers correspond to those in complex **1**, except that the bond lengths and angles are somewhat different. However, due to the different exogenous ligand (pn instead of tn), the connecting modes of the bridging cyanides in **2** are different from those in **1** and this gives rise to some difference in the topologic structures for the two compounds (Figures 2 and 3, right). In complex **2**, the metal atoms W1, Cu1, W2, and Cu2 are linked by four cyano groups (C3−N3, C15−N15, C13−N13, and C4−N4) to form a twelve-membered tetrametallocycle $[\mathrm{Cu_2W_2(CN)_4}]$, and W1, Cu1, W2, and Cu3 are also bridged to form a twelve-membered tetrametallocycle $[\mathrm{Cu_2W_2(CN)_4}]$ by four cyano groups (C3−N3, C10−N10, C11−N11, and C8−N8). By sharing a same lateral (W1−C3−N3−Cu1), the two distorted squares are joined to form a "butterfly-like" motif (Figure 2, left), which is similar to that of **1**. Furthermore, these "butterflies" are connected to each other to lead to one-dimensional spiral chains extended along the *c* axis by sharing one vertex (W2) (Figure 3, right). And then the one-dimensional spiral chains are joined through the CN bridges between W1 and Cu3 to construct the neutral two-dimensional network as shown in Figure 3. The closest metal···metal distances in **1** are 5.267 Å for Cu2···W1 within the layer and 7.104 Å for Cu2···W1″ (″: $1- x, {}^1/_2 + y, {}^1/_2 - z$) between the layers.

Magnetic Properties. The temperature-dependent molar magnetic susceptibilities of **1** were investigated in a magnetic field of 1.0 T (Figure 4). The observed $\chi_M T$ value per $\mathrm{Cu_3W_2}$ unit at 300 K (2.12 $\mathrm{cm^3\ mol^{-1}\ K}$) is in accordance with the expected value (2.06 $\mathrm{cm^3\ mol^{-1}\ K}$) for magnetically isolated three Cu(II) ions ($S = {}^1/_2$, $g = 2.1$)[12] and two W(V) ions ($S = {}^1/_2$, $g = 1.99$).[13] Upon cooling, the $\chi_M T$ value increases slowly until it reaches a maximum of 6.56 $\mathrm{cm^3\ mol^{-1}\ K}$ around 10 K, then decreases abruptly down to 2 K. The magnetic susceptibility above 50 K obeys the Curie−Weiss law for **1**, with a Weiss constant $\theta = +19.52$ K, indicating a ferromagnetic coupling between the adjacent Cu(II)−W(V) magnetic centers within the layer. The χ_M vs T curves of **1** measured at 0.2, 0.7, 1.0, and 2.0 T are shown in the inset of Figure 4, in which the former three curves all show a peak at ca. 11 K, implying a long-range antiferromagnetic (AF) ordering below this point, due to the AF interaction between the ferromagnetic layers. The AF transition is further evidenced by the in-phase zero-field *ac* magnetic susceptibilities $\chi_M'(T)$, which has a peak at ca. 10.7 K (T_N) under $H_{ac} = 5$ Oe and frequencies of 111, 199, 355, 633, and 1111 Hz. No detected out-of-phase signal and frequency dependence were observed, excluding any ferromagnetic and glass behavior (Figure 5). The χ_M value measured at 2.0 T does not show a maximum around 11 K, but increases continuously with the decrease of temperature, indicative of the metamagnetism of complex **1**.

The field dependence of the magnetization (0−7 T) for **1** measured at 1.8 and 9.1 K below T_N (10.7 K) exhibits a pronounced sigmoidal shape (Figure 6). This confirms the metamagnetic behavior of **1**. Below ∼1.25 T, the magnetization increases slowly with increasing field; then it increases abruptly to a ferromagnetic state and reaches a saturation magnetization above 6.5 T. The saturation magnetization at 7.0 T (1.8 K) is 5.0 $N\beta$ per $\mathrm{Cu_3W_2}$ unit, close to the value of 5.14 $N\beta$ anticipated for magnetically isolated three Cu(II) ions ($S = {}^1/_2$, $g = 2.1$) and two W(V) ions ($S = {}^1/_2$, $g = 1.99$). The critical field (the lowest field which is

---

[12] Zheng, L.-M.; Gao, S.; Song, H.-H.; Decurtins, S.; Jacobson, A. J.; Xin, X.-Q. *Chem. Mater.* **2002**, *14*, 3143.

[13] Hayes, R. G. *J. Chem. Phys.* **1966**, *44*, 2210.

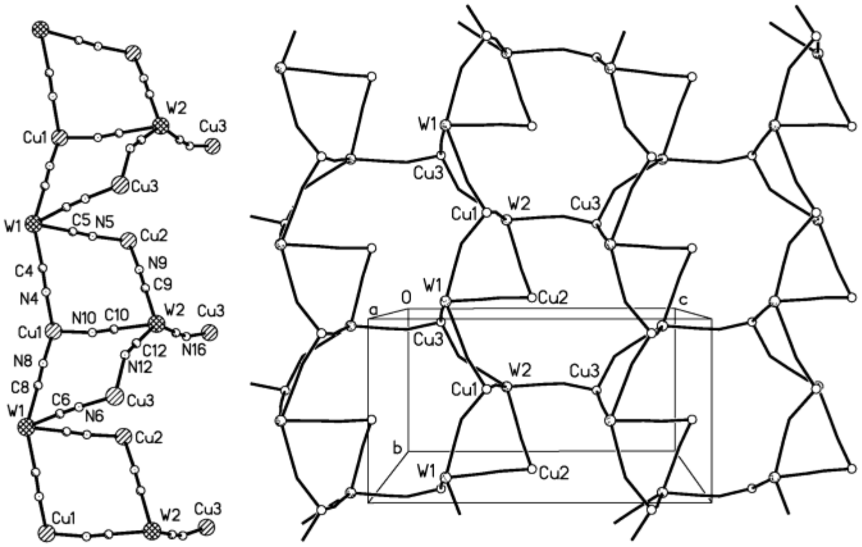

Figure 2. (left) A fragment of **1** along the *b* axis, showing the "butterfly-like" structure. (right) Perspective view of the two-dimensional structure of **1** onto the *bc* plane. The tn ligands and nonbridging CN groups are omitted for clarity.

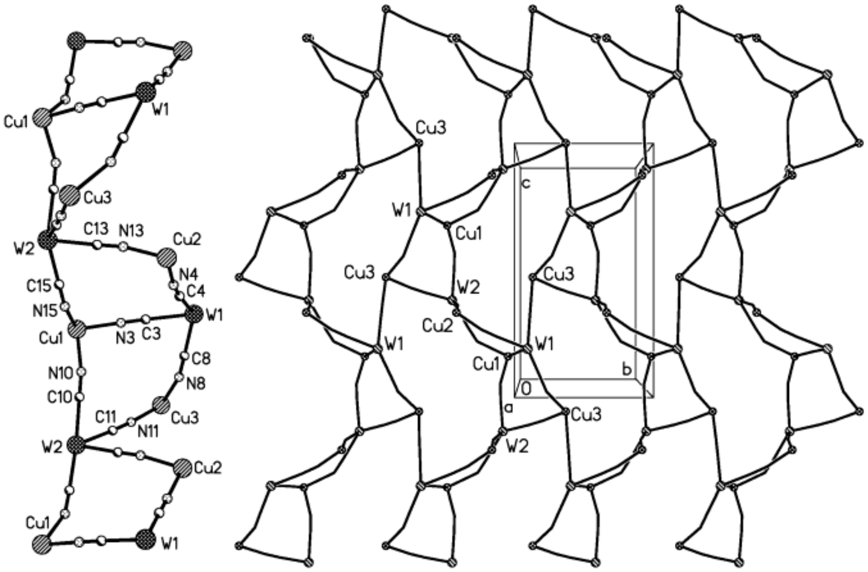

Figure 3. (left) A fragment of **2** along the *c* axis, showing the "butterfly-like" structure. (right) Perspective view of the two-dimensional structure of **2** onto the *bc* plane. The pn ligands and nonbridging CN groups are omitted for clarity.

used to reverse the interlayer antiferromagnetic interaction) is ca. 1.25 T at 1.8 K, and no evident hysteresis loop was observed at 1.8 K.

Similar to that of **1**, the ferromagnetic behavior and metamagnetism are also observed for complex **2**. The χ_M and $\chi_M T$ vs T (2−300 K) plots for **2**, measured in a field of 1.0 T, are shown in Figure 7. The $\chi_M T$ value (per Cu_3W_2) at 300 K is 2.08 cm^3 mol^{-1} K, very close to the spin-only value 2.06 cm^3 mol^{-1} K for three Cu(II) ions ($S = {}^1/_2$, $g = 2.1$) and two W(V) ions ($S = {}^1/_2$, $g = 1.99$), which increases smoothly with decreasing temperature down to 50 K. With a further decrease in temperature, $\chi_M T$ increases sharply, reaching a maximum value of 14.22 cm^3 mol^{-1} K at 8.2 K, and then decreases abruptly down to 2 K. The magnetic susceptibility above 50 K obeys the Curie−Weiss law with a positive Weiss constant, θ, of +28.52 K, which suggests the occurrence of ferromagnetic coupling between the adjacent Cu(II) and W(V) ions. The magnetic susceptibilities of **2** measured in a 200-Oe field show a sharp peak at ca. 8 K (inset of Figure 7), indicating a long-range antiferromagnetic (AF) ordering due to the AF interaction

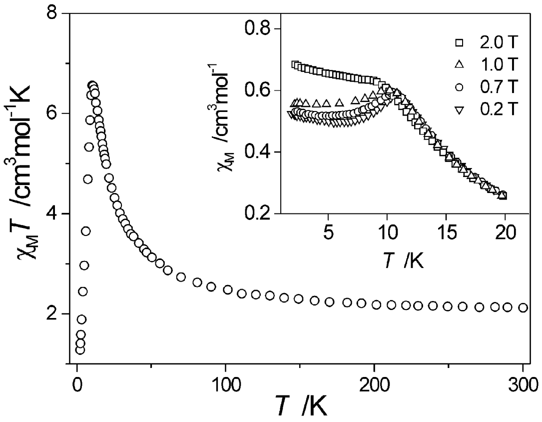

Figure 4. Temperature dependence of $\chi_M T$ for **1** measured at 1.0 T. Inset: Temperature dependence of χ_M in an applied field of 0.2, 0.7, 1.0, and 2.0 T for **1**.

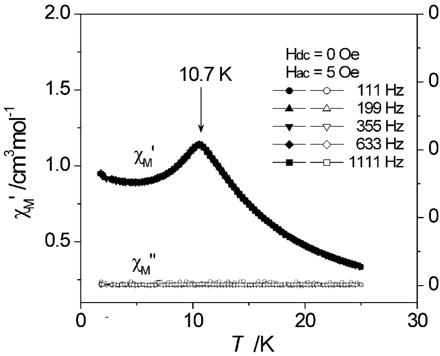

Figure 5. Temperature dependence of *ac* magnetic susceptibilities taken at 111, 199, 355, 633, and 1111 Hz for **1**.

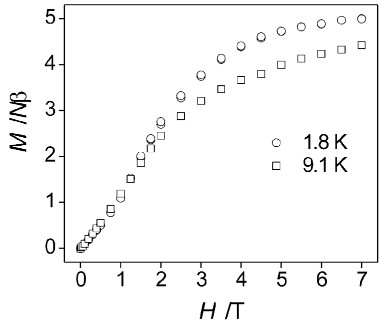

Figure 6. Field-dependent magnetization at 1.8 and 9.1 K for **1**.

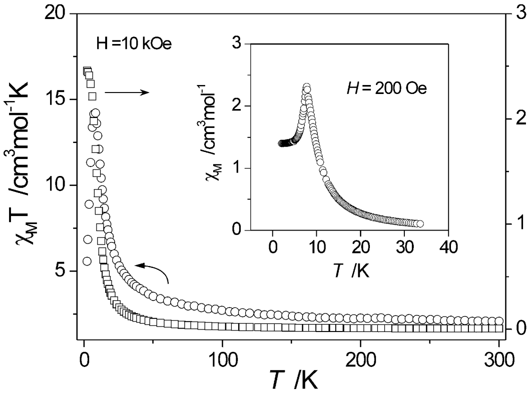

Figure 7. Temperature dependence of $\chi_M T$ and χ_M for **2** measured at 1.0 T. Inset: Temperature dependence of χ_M in an applied field of 200 Oe for **2**.

between the ferromagnetic layers. The temperature dependence of the *ac* magnetic susceptibilities verifies the magnetic phase transition at ca. 8.1 K (T_N) and the absence of a frequency dependence (Figure 8).

The field dependence of the magnetization measured at 1.8 K shown in Figure 9 reveals a hysteresis loop with a coercive field of ca. 70 Oe and remnant magnetization of ca. 0.015 $N\beta$, suggesting that complex **2** is a soft magnet. The magnetization shows a sigmoidal behavior, which suggests metamagnetism for complex **2**. The magnetization first increases slowly with the increasing field and then sharply showing a spin-flipping from an antiferromagnetic arrangement to a ferromagnetic arrangement between the ferromagnetic layers. The magnetization reaches a plateau of 5.11 $N\beta$ per Cu_3W_2 at 4 T, which is in good agreement with the spin-only value of 5.14 $N\beta$ for magnetically isolated Cu_3W_2 unit. The critical field is ca. 0.35 T at 1.8 K.

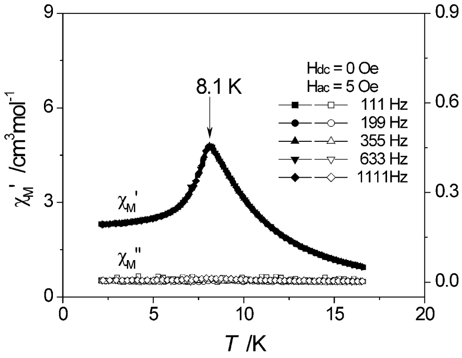

Figure 8. Temperature dependence of *ac* magnetic susceptibilities taken at 111, 199, 355, 633, and 1111 Hz for **2**.

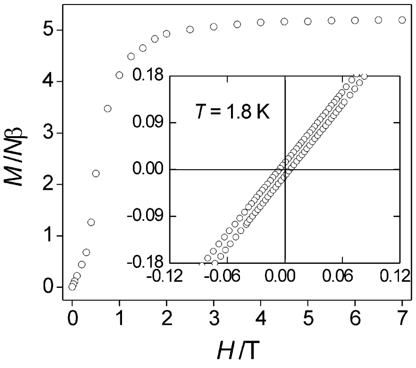

Figure 9. Field-dependent magnetization and hysteresis loop (inset) at 1.8 K for **2**.

In conclusion, the structures and magnetic properties of two novel Cu(II)−W(V) cyano-bridged polymers $[Cu(tn)]_3[W(CN)_8]_2\cdot 3H_2O$ (**1**) and $[Cu(pn)]_3[W(CN)_8]_2\cdot 3H_2O$ (**2**) have been reported in this work. The X-ray structural analysis reveals that the two complexes have a similar layered two-dimensional structure. The cryomagnetic studies demonstrate that both of them show a dominant ferromagnetic behavior within the layer, and the weak interlayer antiferromagnetic interaction gives rise to a metamagnetic behavior below 10.7 K for **1** and 8.1 K for **2** under low field. When a critical field (1.25 T for **1** and 0.35 T for **2**) is reached, the complexes switch from an AF ground state to a ferromagnetic state.

Acknowledgment. Support from the National Natural Science Foundation of China is gratefully acknowledged.

CM030144N